Published in final edited form as:

FASEB J. 2021 March ; 35(3): e21382. doi:10.1096/fj.202002013RR.

Tumor Necrosis Factor-α promotes and exacerbates calcification in heart valve myofibroblast populations

Andrea Gonzalez Rodriguez[1,2], **Megan E. Schroeder**[2,3], **Joseph C. Grim**[1,2], **Cierra J. Walker**[2,3], **Kelly F. Speckl**[1], **Robert M. Weiss**[4], **Kristi S. Anseth**[1,2,3]

[1]Department of Chemical and Biological Engineering, University of Colorado Boulder, Boulder, CO 80303, USA

[2]BioFrontiers Institute, University of Colorado Boulder, Boulder, CO 80309, USA

[3]Materials Science and Engineering Program, University of Colorado Boulder, Boulder, CO 80303

[4]Department of Internal Medicine, University of Iowa, Iowa City, IA, 52242

Abstract

Pro-inflammatory cytokines play critical roles in regulating valvular interstitial cell (VIC) phenotypic changes that can cause heart valve fibrosis and calcification. Tumor necrosis factor alpha (TNF-α) is a cytokine known to influence VIC behavior and has been reported at high levels in calcified valves *ex vivo*. We sought to understand the specific effects of TNF-α on VIC phenotypes (e.g., fibroblast, pro-fibrotic activated myofibroblasts) and its link with heart valve disorders. We characterize human aortic valve tissue from patients with valve disorders and identify a high variability of fibrotic and calcific markers between tissues. These results motivated *in vitro* studies to explore the effects of TNF-α on defined VIC fibroblasts and pro-fibrotic activated myofibroblasts, induced via FGF-2 and TGF-β1 treatment. Using 3D hydrogels to culture VICs, we measure the effect of TNF-α (0.1–10 ng/mL) on key markers of fibrosis (e.g., αSMA, COL1A1) and calcification (e.g., RUNX2, BMP2, calcium deposits). We observe calcification in TNF-α-treated VIC activated myofibroblasts and identify the MAPK/ERK signaling cascade as a potential pathway for TNF-α mediated calcification. Conversely, VIC fibroblasts respond to TNF-α with decreased calcification. Treatment of VIC pro-fibrotic activated myofibroblast populations with TNF-α leads to increased calcification. Our *in vitro* findings correlate with findings in diseased human valves and highlight the importance of understanding the effect of cytokines and signaling pathways on specific VIC phenotypes. Finally, we reveal MAPK/ERK as a potential pathway involved in VIC-mediated matrix calcification with TNF-α treatment, suggesting this pathway as a potential pharmaceutical target for aortic valve disease.

JSC Biotechnology Center, Campus Box 596, Boulder, CO 80309-0596, Phone: 303-492-3147, Fax: 303-492-8425, kristi.anseth@colorado.edu.

Authors Contributions: A. Gonzalez Rodriguez, M. E. Schroeder, J. C. Grim, C. J. Walker and K. S. Anseth designed research; A. Gonzalez Rodriguez, M. E. Schroeder and K. F. Speckl performed research; M. E. Schroeder, C. J. Walker contributed new reagents or analytic tools; A. Gonzalez Rodriguez and C. J. Walker analyzed data; A. Gonzalez Rodriguez wrote the paper; J. C. Grim, R. M. Weiss and K. S. Anseth provided significant revisions and edits to the manuscript.

Conflict of Interest: None

Introduction

Aortic valve stenosis (AVS) is a progressive disease characterized by fibrotic and calcific remodeling and thickening of valve leaflets[1–3]. AVS remains one of the most prevalent heart disorders in developed countries, affecting ~3% of the population over 65 years of age[4–6]. With its high mortality rate[7,8] and lack of effective medical therapies, aortic valve replacement remains the primary clinical treatment; however, many patients are ineligible for surgery. For this reason, a more thorough understanding of the mechanisms that lead to AVS are sought, especially towards the goal of identifying potential targets for therapeutic intervention.

Valvular interstitial cells (VICs) are the main cell population residing in heart valves and are responsible for maintaining valve function and homeostasis. VICs exist primarily as quiescent fibroblasts, but may transition to an activated, pro-fibrotic, myofibroblast phenotype to remodel the extracellular matrix (ECM) in response to injury. This transition is mediated by many factors, including changes in the stiffness of the local microenvironment[9–11] and secreted biochemical cues (e.g., pro-inflammatory cytokines and growth factors) that are known to play critical roles in regulating disease progression[3,12–16]. Among these biochemical cues, transforming growth factor beta 1 (TGF-β1), a cytokine secreted by VICs and immune cells is the most widely studied. TGF-β1 is a potent inducer of the activated myofibroblast phenotype[17]. However, the role that other cytokines secreted by resident fibroblasts and immune cells play in modulating VIC phenotype during AVS progression remains elusive.

Macrophages and neutrophils, as well as resident fibroblasts, secrete pro-inflammatory cytokines that help mediate the inflammatory response during AVS[18–20]. Tumor necrosis factor alpha (TNF-α) is secreted by pro-inflammatory macrophages recruited to injured valve tissue[21–25]. Prior studies have reported influence in both fibrosis and calcification. For example, dermal and pulmonary fibroblasts cultured on tissue culture polystyrene (TCPS) showed an antifibrotic response to treatment with TNF-α (1–100 ng/mL), as measured by a decrease in type I collagen synthesis[26–31]. However, in patients with chronic heart failure, increased levels of circulating TNF-α (0.1–10 ng/mL) have been associated with worsened outcomes when an anti-TNF-α therapy was used in clinical trials[32–37]. These results have led to a growing interest to better understand the regulatory role of TNF-α in AVS. Recent studies suggest that TNF-α induces VIC calcification through both apoptotic and osteogenic mechanisms[38–41]. For example, VIC mineralization in human valves depends on apoptotic signaling through death receptor 4 caused by increasing expression of the TNF ligand superfamily member 10 (TNF10 or TRAIL)[42]. Additionally, TNF-α promotes VIC osteogenic differentiation and mineralization though NF-kB signaling[2]. Furthermore, high levels of calcification in human valves have been linked to an increased density of macrophages,[43,44] suggesting that this increased population of immune cells may be responsible for the high levels of TNF-α present in calcified valves[45].

Based on these reports, we were motivated to interrogate the role of TNF-α on VIC phenotype and its involvement in calcification as related to AVS. As a complexity, AVS patients tend to present with phenotypic and pathological markers (e.g., calcification,

fibrosis)[46–48]. It remains unclear if this patient variability is linked to heterogeneity within the valve cell populations and/or variations in cytokines present in the valve microenvironment. If so, this microenvironmental heterogeneity could further exacerbate AVS progression. Despite the positive correlations between TNF-α and AVS progression, how this cytokine influences VIC phenotypes has yet to be explored systematically. Herein, we exploited a valve-mimetic 3D hydrogel culture system to test hypotheses related to how TNF-α may have differential effects on VIC phenotypes. Specifically, we used a 3D PEG hydrogel system capable of degradation via matrix metalloproteinases (MMPs) to culture VICs within an environment that better recapitulates aspects of their native tissue[49]. We first quantify differences in key markers of fibrosis and calcification in human aortic valve leaflet tissues from patients diagnosed with AVS. Next, using our 3D hydrogel system, we assess the effect of TNF-α treatment on fibroblast, activated myofibroblast, and heterogeneous VIC populations. Changes in key fibrotic markers are characterized through immunostaining, as well as protein and gene expression, to assess the anti-fibrotic effects of TNF-α on VIC phenotypes. We investigate potential pro-calcific effects of TNF-α treatment on VICs by evaluating calcium deposition via histological staining, gene expression, and protein expression for key calcific markers. Finally, we identify potential molecular pathways involved in calcification with TNF-α-treated activated myofibroblasts and identify the MAPK/ERK pathway as a potential target for future therapies.

Materials and methods

Valvular interstitial cell (VIC) isolation and expansion

Male porcine hearts were obtained from Hormel Foods Corporation (Austin, MN, USA) within 24 hours of slaughter. All three layers of aortic valve leaflets (half most distal from the root) were excised from porcine hearts. Leaflets were then washed with Earle's Balanced Salt Solution (Sigma-Aldrich), and digested in 2 mg/mL of Collagenase Type II solution (Worthington Biochemical Corporation) for 30 min to remove endothelial cells, vortexed and digested for an additional 70 min. Samples were then vortexed and filtered with a 100 μm cell strainer to remove any remaining tissue. Freshly isolated VICs were resuspended and plated for expansion in media M199 (Thermo Fisher Scientific) supplemented with 15% fetal bovine serum (FBS, Thermo Fisher Scientific), 1.2 % Penicillin-Streptomycin (Thermo Fisher Scientific) and 0.4% Amphothericin B (Thermo Fisher Scientific).

Material Synthesis

Eight-armed 40 kDa poly(ethylene glycol) (PEG) was functionalized with norbornene as previously described[50]. In brief, amine terminated 40 kDa PEG (JenKem) was reacted with 48 molar equivalents of 5-norbornene-2-carboxylic acid (Sigma-Aldrich) using 40 molar equivalents of O-(7-Azabenzotriazol-1-yl)-N,N,N',N'-tetramethyluronium hexafluorophosphate (HATU, Chem- Impex Intl. Inc.) and 80 molar equivalents of N,N-Diisopropylethylamine (DIEA, Sigma-Aldrich) in N,N-Dimethylformamide (DMF, Fisher Scientific) overnight at room temperature. Product was then precipitated dropwise into cold ethyl ether (VWR), centrifuged to decant off the supernatant, before being washed a second time in ether. Product was dried under vacuum, resuspended in deionized (DI) water, and dialyzed in DI H_2O prior to lyophilization. The extent of end-group functionalization was

confirmed by proton nuclear magnetic resonance imaging to be ~88%; 1H NMR (400MHz, CDCl3, δ): 6.25–5.95 (m, 2H), 3.85–3.25 (m, PEG, 260H).

Cell encapsulation

VICs were encapsulated within 3D MMP-degradable PEG hydrogels via photo-initiated thiol-ene polymerization at a density of 10 million cells/mL. The polymer precursor solution was prepared with 8-arm 40kDa PEG norbornene ([enes]= 6 mM), lithium phenyl-2,4,6-trimethylbenzoylphosphinate ([LAP]= 1.7 mM), CRGDS adhesive peptide ([thiols]= 1 mM, Bachem), and peptide crosslinker KCGPQG↓IWGQCK ([thiols]= 3.34 mM, Bachem, arrow denotes cleavage site) for a thiol:ene ratio of 0.8. The polymer precursor solution was adjusted to a final pH of ~7 with sterile NaOH (1M, Fisher Scientific), mixed with the cell solution and polymerized for 3 min under 365 nm 2.5 mW/cm^2 light to form hydrogel discs 1 mm in height and 6 mm in diameter. Upon reaction, the final swollen storage modulus was 511 ± 140 Pa for all encapsulation studies. After polymerization hydrogels were soaked in 10% FBS M199 and immediately placed in appropriate cell culture medium condition.

3D VIC culture

After encapsulation, VICs were immediately placed in 700 μL of 10% FBS M100, alone or supplemented with 100 ng/mL of FGF-2 (Sigma-Aldrich), 5 ng/mL of TGF-β1 (R&D Systems), or 0.1, 1, or 10 ng/mL of TNF-α (R&D Systems). Media was refreshed every 48 hours with appropriate treatment. For fibroblast-inducing conditions, VICs were cultured for 5 days with FGF-2 (100 ng/mL), while activated myofibroblasts were induced via culture with TGF-β1 (5 ng/mL) for 5 days. For TNF-α-treated fibroblast and activated myofibroblast conditions, fibroblast and activated myofibroblast inducing media were supplemented with TNF-α (10 ng/mL) at day 5.

Material characterization

Swollen hydrogel mechanical properties were characterized with the use of a DHR3 rheometer (TA instruments). Frequency and strain sweeps were performed on equilibrium swollen hydrogels (diameter ~8mm) at 37 °C using an 8 mm Peltier Plate tool covered with adhesive 600/P1200 sandpaper to prevent hydrogel slippage.

Immunostaining for αSMA, actin filaments and nuclei

VIC-laden hydrogels were fixed at room temperature in 10% formalin (Sigma-Aldrich) for 30 min at room temperature and washed with phosphate-buffered saline (PBS, Thermo Fisher Scientific). Cells were then permeabilized for 1 hour using 0.1% Tritonx100 (Fisher Scientific) in PBS and blocked with 5% bovine serum albumin (BSA, Sigma-Aldrich) in PBS for 1 hour at room temperature. Primary mouse monoclonal anti-alpha smooth muscle actin (αSMA, Abcam) was added at 1:1000 in 5% BSA in PBS overnight at 4 °C. Samples were then washed with 0.05% Tween 20 (Sigma-Aldrich) in PBS, and secondary antibody goat-anti-mouse Alexa Fluor 488 (Abcam, 1:300), cytoplasm stain HCS CellMask Orange (Thermo Fisher Scientific, 1:5000) and nucleus label 4’,6-Diamidino-2-Phenylindole (DAPI, Thermo Fisher Scientific, 1:1000) in 5% BSA in PBS were added overnight at 4 °C.

Histological staining for fibrotic and calcific markers

Human valve tissue samples were obtained from OriGene Technologies Inc. Flash frozen tissue section slides were brought to room temperature and fixed with 4% Paraformaldehyde for 12 minutes prior to staining as described below. More details on patient specific information in SI Table 1.

Encapsulated VICs were fixed as previously described, and hydrogels were then soaked in Tissue-Tek® optimum cutting temperature (OCT, VWR) compound for 48 hours at 4 °C. Samples were then embedded in OCT, and 30 μm cryosections were cut using a Cryostat (CM1850, Leica).

Cryosectioned slides were equilibrated to room temperature and soaked in PBS for 10 min to remove OCT. A hydrophobic pen (PAP pen, Fisher Scientific) was used to delineate area of interest and left to dry for 10 min. Alizarin Red was used to stain calcium deposits by adding the Alizarin-Red staining solution (Millipore Sigma) to samples for 5 min. Excess dye was blotted and samples were rinsed in 3 washes of Acetone (Fisher Scientific), followed by 3 washes of a 1:1 ratio of Acetone to Safeclear Xylene Substitute (Fisher Scientific). Finally, samples were rinsed three times in Safeclear for 3 min, excess Safeclear was wiped, and samples were mounted using Permount™ mounting medium (Fisher Scientific).

Von Kossa was used to stain for calcium phosphate; 5% Silver nitrate from the Von Kossa Stain Kit (Abcam) was added to samples and incubated under UV light for 60 min. Samples were then rinsed with running DI water for 1 min. Sodium thiosulfate was subsequently added for 2 min and then rinsed with DI water for 1 min. Nuclear red stain was added for 5 min and rinsed, and samples were then dehydrated by soaking in 95% ethanol solution for 1 min twice, a 100% ethanol solution for 1 min twice, and soaked in Safeclear Xylene substitute solution for 3 min twice before mounting with Permount™ mounting medium.

For the fibrotic markers, αSMA and COL1A1, a procedure was followed that was previously described for immunostaining sectioned hydrogels on slides. Primary mouse monoclonal anti-alpha smooth muscle actin (αSMA, Abcam) was added at 1:1000 in 5% BSA in PBS, and primary mouse monoclonal anti-Collagen I antibody (COL1A1, Abcam) was added at 1:2000 in 5% BSA in PBS. For calcific marker RUNX2, primary rabbit polyclonal anti-runt related transcription factor 2 (RUNX2, Abcam) was added at 1:1000 in 5% BSA in PBS.

RNA isolation and quantitative real-time polymerase chain reaction (RT-qPCR) assessment of gene expression

Hydrogels were digested for 30 min using a 2 mg/mL Collagenase Type II solution. After digestion, the cell solution was centrifuged for 5 min at 1,000 rpm and filtered using a 100 μm cell strainer to remove any remaining hydrogel. Samples were centrifuged again, and the cell pellet was lysed using RLT Buffer (Qiagen) supplemented with 10 μL/mL of 2-mercaptoethanol (Sigma-Aldrich). Total RNA was then isolated using RNeasy Micro Kit (Qiagen), and RNA concentration and quality were assessed with a ND-1000 Nanodrop Spectrophotometer. cDNA was then synthesized using iScript Reverse Transcription

Supermix kit (Bio-Rad) and an Eppendorf Mastercycler. Relative mRNA expression levels were measured with SYBR Green reagents (Bio-Rad) and an iCycler machine (Bio-Rad). Ribosomal protein L30 was used as housekeeping gene to normalize gene expression. Custom primers are presented in Table 1 below:

Calcium deposition assay

Hydrogels were rinsed with PBS, flash frozen in liquid nitrogen, and then lyophilized. Samples were resuspended in a 1 M solution of hydrogen chloride (Sigma-Aldrich) for 48 hours at 4 °C. A QuantiChrom™ Calcium Assay Kit (BioAssay Systems) was then used to quantitatively determine the calcium ion Ca^{2+} deposited by VICs, following manufacturer instructions and measuring absorbance at 612 nm.

Caspase 3/7 fluorescence assay

Encapsulated VICs were treated with an 8 μM solution of CellEvent™ Caspase-3/7 Green Detection Reagent (Thermo Fisher Scientific) in PBS with 5% FBS for 1 hour at 37 °C. Fluorescence levels were then measured using a Plate Reader Tecan Infinite M200 at excitation/emission spectrums of 502/530 nm.

Western blots

Protein lysate was collected from hydrogels by digesting samples as described for RNA samples, and the cell pellet was resuspended in RIPA buffer (ThermoFisher Scientific) supplemented with Protease/Phosphatase inhibitor and EDTA (ThermoFisher Scientific, 1:100). Chemiluminescence western blot techniques were then used to assess αSMA protein expression relative to total protein levels (Ponceau stain, LI-COR Biosciences). Protein electrophoresis was run in 4–20% Mini-PROTEAN® TGX™ precast gels (Bio-Rad) and transferred to poly (vinylidene difluoride) (PDVF) membranes (Bio-Rad). Samples were probed using primary αSMA antibody (Abcam, 1:2000) diluted in 5% milk in TBST overnight at 4 °C. Membranes were then incubated with secondary goat-anti-mouse HRP conjugated antibody (Jackson ImmunoResearch, 1:10000) diluted in 5% milk in TBST for 1 hour at room temperature. Chemiluminescence signal was detected using Pierce ECL Plus solution (ThermoFisher Scientific) and ImageQuant LAS 4000 detector.

Microscopy and analysis

Images were acquired via a Nikon Ti-E Spinning Disc Confocal, a confocal Zeiss Laser Scanning Microscope 710 or a Nikon Eclipse TE300 microscope. Image analysis was performed with Microscopy Imaging Analysis Software (Bitplane) or FIJI[51].

Statistical analysis

Data are presented as mean ± standard deviation (SD) with a minimum of three biological and technical replicates for all studies. For human tissues, statistical analysis was performed on fields of view for each biological replicate ($n \geq 10$ images per biological replicate). Data were analyzed by t-test or analysis of variance (ANOVA) using Graph pad™ (Prism).

Ethics

No special approvals were required for the VICs or human tissue samples used in these studies.

Results

Human stenotic valves display variable and heterogeneous fibrotic and calcific markers

We first examined aortic valve tissue from male patients diagnosed with heart valve disorder to better understand the level of heterogeneity that can arise in valve cell populations (SI Table 1). We observed both fibrotic and calcific markers via immunofluorescence staining. Alpha smooth muscle actin (αSMA) and Collagen Type I alpha 1 (COL1A1) were used as nominal markers associated with fibrosis (Figure 1a–b). Histological analysis for αSMA demonstrated significant differences between tissues, suggesting heterogeneity in the myofibroblast populations (Figure 1f). When COL1A1 intensity was quantified, we also observed differences amongst tissues, albeit non-significant (Figure 1g). Besides key differences between tissues, all were positive for αSMA and COL1A1, suggesting the presence of pro-fibrotic myofibroblasts in stenotic patients.

Next, tissue sections were stained for the calcific markers: runt-related transcription factor 2 (RUNX2) via immunofluorescence and Von Kossa and Alizarin Red for mineralization (Figure 1c–e). RUNX2 intensity was statistically different between the tissue samples (Figure 1h); RUNX2 is an early osteogenic marker. Alizarin red staining is a direct measure of calcium deposition, while Von Kossa stains for calcium phosphates (e.g., hydroxyapatite) and correlates with the levels of valve tissue calcification. Both stains provide insight into the severity of calcification in the tissue and together they provide complementary evidence of mineralization deposition within the matrix. With Von Kossa and Alizarin Red staining, we clearly observe different amounts of black (calcium phosphate) and red (calcium deposits) staining between tissues, which indicates different levels of calcification amongst patients with the same diagnosis. We further quantified the area of the valve that was calcified (i.e., percentage of positive Von Kossa staining in the image, (Figure 1i)), and these results further highlight the variability observed in calcification severity, as well as regional areas of calcification within valve tissue from the same patient. Collectively, these results suggest significant variability exists in fibrotic and calcific markers in human patients with the same diagnosis; thus, supporting our hypothesis that there are likely variable and heterogenous VIC phenotypes present in diseased valve tissue.

TNF-α treatment decreases expression of fibrotic markers in VIC cultures

We next investigated whether TNF-α would have pro- or anti-fibrotic effects on VICs cultured within a 3D environment that recapitulates key aspects of the valve matrix. Specifically, VICs were encapsulated within a matrix metalloprotease (MMP)-degradable poly(ethylene glycol)(PEG) hydrogel with a fibronectin mimic adhesive ligand, RGD (Figure 2a). Prior results demonstrate that this hydrogel platform can modulate the fibroblast phenotype of VICs[52], thus enabling us to explore systematically how TNF-α influences VIC phenotype. First, VICs were encapsulated in these peptide functionalized PEG gels and cultured in the presence of various concentrations of TNF-α (0.001, 0.01, 0.1, 1, 10 and 100

ng/mL) for 10 days. αSMA protein expression was assessed and compared to controls (Figure 2d). Treatment of encapsulated VICs with TNF-α concentrations ≥ 10 ng/mL resulted in a significant decrease in αSMA protein expression. Human serum has TNF-α levels between 0.1 – 10 ng/mL[53–58], suggesting our findings are consistent with physiologically-relevant concentrations of TNF-α.

We next studied whether TNF-α would also decrease αSMA stress fiber formation, which we measured via immunostaining (Figure 2b). We found that increasing TNF-α concentration led to decreases in αSMA stress fiber formation, indicating a decrease in VIC transition from quiescence to myofibroblast activation. This observation was further quantified via αSMA mean intensity analysis, normalized to cell number, and results confirm that high doses of TNF-α concentration (i.e., 1 and 10 ng/mL) significantly decrease VIC activated myofibroblast population. We also assessed the effect of TNF-α on other VIC fibrotic markers, namely mRNA expression levels of αSMA, COL1A1, and CTGF (Figure 2e–f). At all TNF-α treatment concentrations, RT-qPCR showed a significant decrease in αSMA mRNA levels; however, COL1A1 and CTGF were not significantly affected (Figure 2g). In total, our *in vitro* VIC studies document that TNF-α induces an anti-fibrotic VIC phenotype, as measured by αSMA stress fiber formation, gene, and protein expression.

VICs increase expression of calcific markers when treated with TNF-α

Given the high levels of TNF-α observed in calcified aortic valve leaflets relative to healthy valve leaflets from previously published literature[32,45], we were curious as to whether TNF-α induces a pro-calcific VIC phenotype. Encapsulated VICs were treated with 0, 0.1, 1, or 10 ng/mL TNF-α, and samples were evaluated histologically for mineralization via Von Kossa and Alizarin Red staining (Figure 3a). Results show an increase in both calcific marker stains with increasing TNF-α concentration. To further characterize VIC phenotypic changes, mRNA levels of runt-related transcription factor 2 (RUNX2) and bone morphogenic protein 2 (BMP2) were assessed, as common markers for the osteoblast-like phenotype. Significant upregulation in both markers was observed at the highest dose of TNF-α (10 ng/mL) (Figure 3b–c).

TNF-α signaling has been linked to apoptosis-mediated calcification through the activation of Caspase-3, an early marker of apoptosis[42,59]. Hence, we next examined Caspase 3 fluorescence levels in response to TNF-α treatment (10 ng/mL) and observed a significant increase in Caspase-3 signal normalized to dsDNA content (Figure 3d). We also assessed calcium content via a colorimetric assay normalized to dsDNA content and expressed as percent of untreated control but observed no significant differences when treated with either the 1 or 10 ng/mL of TNF-α concentrations (Figure 3e). Interestingly, the lowest TNF-α treatment concentration led to a significant decrease in calcium content within our 3D VIC culture. However, no other concentrations produced a decrease in calcification markers with low concentration of TNF-α. Taken together, we posit that TNF-α promotes calcification by inducing a VIC osteoblast-like phenotype and by increasing VIC apoptosis at high concentrations.

Treatment of VIC activated myofibroblast populations with TNF-α decreases expression of fibrotic markers

Differences observed in the fibroblast-myofibroblast heterogeneity between tissues (Figure 1) suggested to us that TNF-α may be inducing heterogeneous responses, depending on resident VIC phenotype (fibroblast vs. myofibroblast). We hypothesized that fibroblasts *vs.* pro-fibrotic activated myofibroblasts would respond differentially to TNF-α. To test that hypothesis, we used previously identified conditions[52] to create well-defined fibroblast and activated myofibroblast populations via treatment with either FGF-2 (100 ng/mL) or TGF-β1 (5 ng/mL) for 5 days in our 3D hydrogel cultures (SI Figure 1).

Upon generating relatively uniform VIC fibroblast or VIC activated myofibroblasts populations, we then added TNF-α (10 ng/mL) to the cultures (Figure 4a). After 5 days of exposure to TNF- α (Day 10), we then quantified differences in αSMA protein levels via western blots. While non-significant, a decreasing trend in total protein expression was observed with TNF-α treatment for both the fibroblast and activated myofibroblast populations (Figure 4b). We next examined αSMA stress fiber organization (Figure 4c) with TNF-α treatment. The TNF-α treated fibroblast populations had low levels of diffuse αSMA staining, similar to those in the untreated controls. In contrast, TNF-α treated activated myofibroblasts had diffuse αSMA staining, with a significant reduction in stress fibers compared to the untreated controls (which demonstrated high levels of αSMA stress fibers). This decrease in αSMA stress fiber formation suggested to us a potential anti-fibrotic role of TNF-α in mediating VIC phenotype. This was further characterized by quantification of the αSMA mean intensity normalized to cell number (Figure 4d), which confirmed a significant decrease in αSMA expression in TNF-α-treated activated myofibroblasts. VIC fibroblasts populations had no significant differences between the TNF-α treated samples and controls. With respect to mRNA expression levels (Figure 4e–f), αSMA and COL1A1 were similar in both TNF-α treated and untreated VIC fibroblasts, but significantly decreased in VIC activated myofibroblast phenotype treated with TNF-α. Together, these results suggest an antifibrotic effect of TNF-α on VIC activated myofibroblast populations, with little effect on the quiescent VIC fibroblast phenotype. Thus, revealing a mechanistically dichotomous impact of TNF-α on VICs depending on their phenotype.

VIC activated myofibroblast populations respond to TNF-α treatment with increased expression of calcific markers

We next explored the effect of TNF-α treatment on the expression of calcific markers, using the same experimental design on well-defined VIC fibroblast *vs.* activated myofibroblast populations (Figure 5a). First, the amount of calcium deposition in response to TNF-α treatment was quantified, normalized to dsDNA and expressed as percent of the untreated fibroblast condition (Figure 5b). Interestingly, VIC fibroblasts exhibited a 30% decrease in calcium deposition with TNF-α treatment, while the VIC activated myofibroblast phenotype significantly increased calcium deposition by 60%. Next, we stained for calcium (Alizarin Red) and calcium phosphate (Von Kossa) depositions in histological sections of VIC-laden hydrogels (Figure 5c) for both conditions. Visually, no differences were observed in the fibroblasts with and without TNF-α treatment, but on the contrary, activated myofibroblast

had increased positive staining of both calcium and calcium phosphate in the presence of TNF-α.

To further investigate these different cellular responses, we analyzed mRNA levels of calcific gene markers, RUNX2 and BMP2 (Figure 5d–e) in response to the TNF-α treatment. RUNX2 and BMP2 gene expression decreased in the quiescent fibroblast phenotype with TNF-α treatment. Conversely, RUNX2 significantly increased 5-fold and BMP2 increased 3.6-fold in the activated myofibroblast populations with TNF-α treatment. Again, we investigated the effect of TNF-α on Caspase 3 levels (Figure 5f) normalized to dsDNA content for each condition. Consistent with our finding, TNF-α treatment led to a significant decrease in Caspase 3 activity in the quiescent fibroblast phenotype, while activated myofibroblasts had a 1.4-fold increase in Caspase 3 activity. Combined, these results highlight that the VIC phenotype (i.e., fibroblast or myofibroblast) influences its response to the same pro-inflammatory cytokine, TNF-α.

TNF-α induced calcific response in VIC activated myofibroblasts involves MAPK/ERK signaling

Finally, we investigated potential molecular mechanisms involved in the VIC activated myofibroblast calcific response to TNF-α treatment. Since the MAPK/ERK pathway is known to mediate TNF-α signaling[60], we first tested if perturbation of ERK signaling through MEK1/2 inhibition would abrogate TNF-α's effect on VIC activated myofibroblast. VICs were encapsulated in MMP-degradable hydrogels under conditions that induced their myofibroblast activation for 5 days, and then treated with TNF-α in the presence or absence of Selumetinib (MEK1/2 inhibitor[61]) (Figure 6). The concentrations of Selumetinib were chosen based on efficacy after 3 days (SI Figure 2). Changes in fibrotic and calcific gene expression markers were measured via RT-qPCR (Figure 6a–c). Selumetinib resulted in significant upregulation of αSMA and downregulation of RUNX2 gene expression at 10 μM, while no statistically significant differences were observed in BMP2 gene expression. When comparing the effects of Selumetinib at 10 μM on activated myofibroblast cultured with TNF-α (Figure 6c), we observed an ~18.5-fold increase for αSMA, ~60% decrease for RUNX2 and ~30% decrease for BMP2 gene expression. Other molecular pathways that have been implicated in TNF-α signaling, including AMPK and PKA activation [62,63], were investigated but no significant effects were observed with respect to expression of either fibrotic and calcific genes (SI Figure 3). These results suggest that inhibition of the MAPK/ERK signaling pathway may be able to prevent calcification caused by TNF-α in VIC activated myofibroblast populations, while also reverting their anti-fibrotic potential.

Discussion

The role of TNF-α in AVS progression remains elusive, with discussion over its anti-fibrotic[26–30] and pro-calcific[38–40] effects. The inconclusive results are likely due to the heterogeneity in cell population within diseased valves. The present study demonstrates that there is high variability in markers for fibrosis and calcification across diseased human valve samples. This heterogeneity might also be partly responsible for the failed clinical trials regarding anti-TNF-α therapeutics for fibrosis in other disease states[32–37]. Therefore, we

strove to systematically test the fibrotic and calcific role of TNF-α in 3D tissue-mimicking hydrogel culture scaffolds[49]. Our findings indicate disparate effects of TNF-α treatment on quiescent fibroblast *vs.* activated myofibroblast VIC populations, playing anti-fibrotic and pro-calcific roles, respectively. Moreover, we show that the ERK/MAPK pathway plays a role in TNF-α induced calcification of VIC activated myofibroblasts. Ultimately, these findings imply that AVS treatments may need to be tailored to the individual patient, taking into consideration the composition of VIC phenotype.

AVS is an active and cell-mediated disease process in which resident VICs can transition between their fibroblast and activated myofibroblasts phenotypes to modulate disease progression[1]. The ratio of activated myofibroblasts to quiescent fibroblasts likely plays an important role in disease progression and is one indicator of AVS severity. Our observations of diseased human valve tissue point towards a correlation between high levels of fibrotic markers and increased calcification severity (Figure 1). However, we identified significantly different levels of fibrosis and calcification between tissues despite their same diagnosis, indicating a vast range of disease phenotypes categorized under “aortic valve disease”. Future studies assessing valve tissue at the gene and protein level across a wide range of patients and disease severity would help researchers understand the heterogeneity of AVS progression, identify basal levels of fibrotic and calcific markers, and develop more patient-specific treatments.

The opposing fibrotic and calcific response between activated myofibroblasts and fibroblasts to TNF-α treatment could be a key to understanding the widely debated effects of TNF-α. Perhaps anti-TNF-α therapies were unsuccessful because they failed to take into consideration heterogeneous cell phenotype populations. We speculate that other cytokines may act in similar heterogeneous manners, affecting fibroblasts and activated myofibroblasts differently. While some work has focused on identifying differential responses to soluble biochemical cues on VICs cultured on soft and stiff 2D hydrogels[64], which resemble the mechanics of healthy and diseased valves, respectively, more extensive work needs to be done on examining the effects of cytokines on discrete VIC fibroblast and activated myofibroblasts populations. As the ratio of fibroblast to activated myofibroblasts populations shifts with disease progression, a better understanding as to how cytokines and drugs affect individual VIC populations could improve knowledge about AVS progression and help elucidate more specific therapeutic targets. Therefore, the results presented herein identifying the dichotomous effects of TNF-α on quiescent fibroblasts *vs* activated myofibroblasts may have major translational impacts. Another factor to take into consideration is the existing parallels between the differences observed amongst VICs residing in different leaflet layers (i.e., fibrosa, spongiosa and ventricularis) and those between different VIC phenotypes. Previous studies have reported that VICs within the fibrosa layer can be exposed to local factors that promote fibrotic and calcific pathological development[65,66], more representative of that of our activated myofibroblasts in response to TNF-α treatment. However, VICs from the ventricularis layer are more susceptible to pro-fibrotic biochemical stimuli that those from the fibrosa layer[67]. These parallels might suggest the fibrosa layer may be more sensitive to TNF-α mediated calcification than the venticularis layer. Overall, the results presented herein indicate impactful implications between our results and how different layers of the valve respond to TNF-α.

The disparity in results as to the role of TNF-α in AVS could be related to its influence on VIC phenotype. While the presence of TNF-α in calcified valves may be indicative of its pro-calcific effects, others have identified TNF-α as a key mediator of VIC myofibroblast deactivation. Recent work reported increased levels of TNF-α in serum from patients after receiving transcatheter valve replacement (TAVR)[64]. When analyzing the effects of post-TAVR serum on VICs cultured on soft and stiff hydrogels, TNF-α was one of the main drivers for decreases in VIC αSMA stress fiber formation, a hallmark of VIC activated myofibroblasts. Similarly, decreases in αSMA stress fiber formation, mRNA expression, and collagen synthesis have been observed in quiescent fibroblasts upon treatment with TNF-α[26,64]. Our observations are consistent with these results and point towards an anti-fibrotic role of TNF-α on primarily quiescent VIC fibroblasts (Figure 2). Moreover, previously published work has reported increased expression of pro-calcific markers in response to TNF-α on VICs obtained from patients with AVS. Specifically, reports have linked human valve calcification with TNF-α signaling through the activation of Caspase 3, an early apoptotic marker[42,59]. Our findings with histological staining of mineral deposits, gene expression of pro-calcific markers, and Caspase 3 activity (Figure 3) align with these studies and suggest apoptosis-mediated calcification occurs within our 3D VIC samples with TNF-α treatment. However, total calcium deposition levels within our 3D substrates was not significantly altered between treatment conditions of TNF-α alone. We acknowledge that while increased expression of early pro-calcific markers was observed, no changes in overall macroscopic calcification levels occurred. The inherently bioinert properties of our PEG-based hydrogels could explain the lack of calcium nucleation over the time course of this study, therefore future work should investigate the long-term effects of TNF-α on calcification within a system tailored for mineral nucleation. Interestingly, others have reported parallel effects of TNF-α with increasing fibrotic and calcific markers on murine VICs, but used supraphysiological levels of TNF-α[68]. Here, we were able to identify dichotomous effects of TNF-α on fibrotic and calcific markers within a physiologically relevant TNF-α dose regime, using culture matrices which closely resemble the mechanical properties of valve tissue *in vivo*. Our findings revealed different mechanisms of calcification, specifically changes in osteogenic *vs.* apoptosis-related calcific markers, while previous findings focused on contraction and the presence of nodules.

We found that the MAPK/ERK pathway was involved in TNF-α-mediated increase in calcification, supporting previous studies that demonstrated that this pathway mediates TNF-α signaling in other settings[60] (Figure 6). The small molecule inhibitor Selumetinib can disrupt ERK signaling through MEK1/2 inhibition and lead to a reversal of TNF-α mediated anti-fibrotic and pro-calcific effects on activated myofibroblast populations as assessed by gene expression analysis. Interestingly, Selumetinib is a therapeutic currently used for the treatment of a myriad of different cancers[69–71], with clinical trials assessing its use for other pathologies, such as neurofibromatosis type 1[72], cardiomyopathy, and kidney fibrosis[73,74]. Future studies warrant a deeper exploration of the effects of Selumetinib on VIC phenotype, since we observe dramatic changes in αSMA expression levels and insignificant effects on BMP2 expression. The expression of BMP2 has been shown to be mediated through NF-κB signaling in order to induce valve calcification[75,76]. Since Selumetinib causes complete reversal of calcification, further investigation of the role of ERK signaling within the NF-κB

pathway to promote VIC calcification is warranted[62,77,78]. However, reduced RUNX2 gene expression suggests the potential involvement of the MAPK/ERK pathway in TNF-α induced exacerbated calcification. Our findings reveal MAPK/ERK as a target for valve calcification, and also highlight Selumetinib as a potential therapy for AVS.

The 3D hydrogel scaffolds provided a culture environment that more closely represents VICs in native valve tissue. Supraphysiologically stiff culture platforms (~1 GPa), such as traditional culture polystyrene plates[62], can lead to confounding results due to the nearly 100% activation of VICs into the pro-fibrotic myofibroblast phenotype[79,80]. 2D hydrogel cultures are an improvement in which they match the mechanical properties of the native VIC tissue. However, 3D culture platforms further allow for the study of cell migration, cell-matrix interaction with degradation and contraction of the matrix, and long-term culture. While the use of 3D hydrogels is reagent and cell intensive, these matrices provide specific benefits when studying the VIC phenotype and the response to cytokines in the context of mechanosensing and matrix interactions. Future experiments aimed at validating appropriate *in vitro* models to predict *in vivo* disease progression are on-going and would be an important advancement for the field.

In summary, we used 3D MMP-degradable hydrogels to culture VICs in a manner that better recapitulates their native environment to explore the role of TNF-α signaling on defined fibroblast and pro-fibrotic activated myofibroblast valve populations. Our data uncovered the dichotomous impact of TNF-α upon VICs, as shown by increases in calcification in activated myofibroblasts treated with TNF-α and decreases in overall calcification in fibroblast populations. These findings further highlight the potential importance of valve cell heterogeneity in a patient's response to drug therapeutics for AVS treatment.

Supplementary Material

Refer to Web version on PubMed Central for supplementary material.

Acknowledgements:

We would like to thank L. Leinwand, A. Killaars, V. Rao, T. Ceccato and B. Aguado for thoughtful discussions related to this study.

Sources of funding: The authors would like to thank the NIH for funding research through grants RO1HL132353 and RO1HL142935. JCG acknowledges funding from the NIH (T32 HL007822). CJW acknowledges funding from F31HL142223. KFS acknowledges funding from the Biological Sciences Initiative Fellowship. RMW acknowledges fund from American Heart Association Grant #18IPA34170040.

Nonstandard Abbreviations

AVS	Aortic valve stenosis
VIC	Valvular interstitial cell
TNF-α	Tumor necrosis factor alpha
TGF-β1	Transforming growth factor beta 1
FGF-2	Fibroblast growth factor 2

αSMA	Alpha smooth muscle actin
COL1A1	Collagen type 1 alpha 1
CTGF	Connective tissue growth factor
RUNX2	Runt-related transcription factor 2
BMP2	Bone morphogenetic protein 2
MAPK/ERK	Mitogen-activated protein kinases/Extracellular signal-regulated kinases
ECM	Extracellular matrix
TCPS	Tissue culture polystyrene
PEG	Poly(ethylene glycol)
MMP	Matrix metalloproteinase
dsDNA	double-stranded DNA
TAVR	transcatheter valve replacement

References:

1. Rajamannan NM, Evans FJ, Aikawa E, Grande-Allen KJ, Demer LL, Heistad DD, Simmons CA, Masters KS, Mathieu P, O'Brien KD, Schoen FJ, Towler DA, Yoganathan AP, Otto CM. Calcific aortic valve disease: not simply a degenerative process: A review and agenda for research from the National Heart and Lung and Blood Institute Aortic Stenosis Working Group. Circulation. 2011;124(16):1783–1791. doi:10.1161/CIRCULATIONAHA.110.006767 [PubMed: 22007101]
2. Lindman BR, Clavel M-A, Mathieu P, Iung B, Lancellotti P, Otto CM, Pibarot P. Calcific aortic stenosis. Nat Rev Dis Prim. 2016;2(1):16006. doi:10.1038/nrdp.2016.6 [PubMed: 27188578]
3. Benton JA, Kern HB, Leinwand LA, Mariner PD, Anseth KS. Statins Block Calcific Nodule Formation of Valvular Interstitial Cells by Inhibiting α-Smooth Muscle Actin Expression. Arterioscler Thromb Vasc Biol. 2009;29(11):1950–1957. doi:10.1161/ATVBAHA.109.195271 [PubMed: 19679827]
4. Nkomo VT, Gardin JM, Skelton TN, Gottdiener JS, Scott CG, Enriquez-Sarano M. Burden of valvular heart diseases: a population-based study. Lancet. 2006;368(9540):1005–1011. doi:10.1016/S0140-6736(06)69208-8 [PubMed: 16980116]
5. Chen Y, Yiu KH. Growing importance of valvular heart disease in the elderly. J Thorac Dis. 2016;8(12):E1701–E1703. doi:10.21037/jtd.2016.12.23 [PubMed: 28149618]
6. Yutzey KE, Demer LL, Body SC, Huggins GS, Towler DA, Giachelli CM, Hofmann-Bowman MA, Mortlock DP, Rogers MB, Sadeghi MM, Aikawa E. Calcific aortic valve disease: A consensus summary from the alliance of investigators on calcific aortic valve disease. Arterioscler Thromb Vasc Biol. 2014;34(11):2387–2393. doi:10.1161/ATVBAHA.114.302523 [PubMed: 25189570]
7. Otto CM, Prendergast B. Aortic-Valve Stenosis — From Patients at Risk to Severe Valve Obstruction. N Engl J Med. 2014;371(8):744–756. doi:10.1056/NEJMra1313875 [PubMed: 25140960]
8. O'Brien KD. Pathogenesis of Calcific Aortic Valve Disease. Arterioscler Thromb Vasc Biol. 2006;26(8):1721–1728. doi:10.1161/01.ATV.0000227513.13697.ac [PubMed: 16709942]
9. Kloxin AM, Benton JA, Anseth KS. In situ elasticity modulation with dynamic substrates to direct cell phenotype. Biomaterials. 2010;31(1):1–8. doi:10.1016/j.biomaterials.2009.09.025 [PubMed: 19788947]

10. Quinlan AMT, Billiar KL. Investigating the role of substrate stiffness in the persistence of valvular interstitial cell activation. J Biomed Mater Res Part A. Published online 2012:n/a-n/a. doi:10.1002/jbm.a.34162

11. Yip CYY, Chen JH, Zhao R, Simmons CA. Calcification by valve interstitial cells is regulated by the stiffness of the extracellular matrix. Arterioscler Thromb Vasc Biol. 2009;29(6):936–942. doi:10.1161/ATVBAHA.108.182394 [PubMed: 19304575]

12. Blaser MC, Simmons CA. Mechanical and matrix regulation of valvular fibrosis In: Cardiac Fibrosis and Heart Failure: Cause or Effect?. Advances in Health and Disease. Springer International Publishing; 2015:23–53. doi:10.1007/978-3-319-17437-2_3

13. Walker GA, Masters KS, Shah DN, Anseth KS, Leinwand LA. Valvular Myofibroblast Activation by Transforming Growth Factor-β. Circ Res. 2004;95(3):253–260. doi:10.1161/01.RES.0000136520.07995.aa [PubMed: 15217906]

14. Cushing MC, Mariner PD, Liao J-T, Sims EA, Anseth KS. Fibroblast growth factor represses Smad-mediated myofibroblast activation in aortic valvular interstitial cells. FASEB J. 2008;22(6):1769–1777. doi:10.1096/fj.07-087627 [PubMed: 18218921]

15. Dolivo DM, Larson SA, Dominko T. Fibroblast Growth Factor 2 as an Antifibrotic: Antagonism of Myofibroblast Differentiation and Suppression of Pro-Fibrotic Gene Expression. Cytokine Growth Factor Rev. 2017;38:49–58. doi:10.1016/J.CYTOGFR.2017.09.003 [PubMed: 28967471]

16. Liu AC, Gotlieb AI. Transforming Growth Factor-β Regulates in Vitro Heart Valve Repair by Activated Valve Interstitial Cells. Am J Pathol. 2008;173(5):1275–1285. doi:10.2353/AJPATH.2008.080365 [PubMed: 18832581]

17. Cushing MC, Liao J-T, Anseth KS. Activation of valvular interstitial cells is mediated by transforming growth factor-β1 interactions with matrix molecules. Matrix Biol. 2005;24(6):428–437. doi:10.1016/J.MATBIO.2005.06.007 [PubMed: 16055320]

18. Li G, Qiao W, Zhang W, Li F, Shi J, Dong N. The shift of macrophages toward M1 phenotype promotes aortic valvular calcification. J Thorac Cardiovasc Surg. 2017;153(6):1318–1327.e1. doi:10.1016/j.jtcvs.2017.01.052 [PubMed: 28283241]

19. Wypasek E, Natorska J, Grudzień G, Filip G, Sadowski J, Undas A. Mast cells in human stenotic aortic valves are associated with the severity of stenosis. Inflammation. 2013;36(2):449–456. doi:10.1007/s10753-012-9565-z [PubMed: 23108956]

20. Calin MV, Manduteanu I, Dragomir E, Dragan E, Nicolae M, Gan AM, Simionescu M. Effect of depletion of monocytes/macrophages on early aortic valve lesion in experimental hyperlipidemia. Cell Tissue Res. 2009;336(2):237–248. doi:10.1007/s00441-009-0765-2 [PubMed: 19301037]

21. Kaden JJ, Dempfle CE, Grobholz R, Fischer CS, Vocke DC, Kiliç R, Sarikoç A, Piñol R, Hagl S, Lang S, Brueckmann M, Borggrefe M. Inflammatory regulation of extracellular matrix remodeling in calcific aortic valve stenosis. Cardiovasc Pathol. 2005;14(2):80–87. doi:10.1016/j.carpath.2005.01.002 [PubMed: 15780799]

22. Jovinge S, Ares MPS, Kallin B, Nilsson J. Human monocytes/macrophages release TNF-α in response to Ox-LDL. Arterioscler Thromb Vasc Biol. 1996;16(12):1573–1579. doi:10.1161/01.ATV.16.12.1573 [PubMed: 8977464]

23. Hershkoviz R, Cahalon L, Gilat D, Miron S, Miller A, Lider O. Physically Damaged Extracellular Matrix Induces TNF-alpha Secretion by Interacting Resting CD4+ T Cells and Macrophages. Scand J Immunol. 1993;37(1):111–115. doi:10.1111/j.1365-3083.1993.tb01672.x [PubMed: 8093416]

24. Mizutani H, Ohmoto Y, Mizutani T, Murata M, Shimizu M. Role of increased production of monocytes TNF-α, IL-1β and IL-6 in psoriasis: Relation to focal infection, disease activity and responses to treatments. J Dermatol Sci. 1997;14(2):145–153. doi:10.1016/S0923-1811(96)00562-2 [PubMed: 9039978]

25. Goody PR, Hosen MR, Christmann D, Niepmann ST, Zietzer A, Adam M, Bönner F, Zimmer S, Nickenig G, Jansen F. Aortic valve stenosis: From basic mechanisms to novel therapeutic targets. Arterioscler Thromb Vasc Biol. 2020;40:885–900. doi:10.1161/ATVBAHA.119.313067 [PubMed: 32160774]

26. Fujita M, Shannon JM, Morikawa O, Gauldie J, Hara N, Mason RJ. Overexpression of Tumor Necrosis Factor-α Diminishes Pulmonary Fibrosis Induced by Bleomycin or Transforming Growth

Factor-β. Am J Respir Cell Mol Biol. 2003;29(6):669–676. doi:10.1165/rcmb.2002-0046OC [PubMed: 12816730]

27. Yamane K, Ihn H, Asano Y, Jinnin M, Tamaki K. Antagonistic effects of TNF-alpha on TGF-beta signaling through down-regulation of TGF-beta receptor type II in human dermal fibroblasts. J Immunol. 2003;171(7):3855–3862. doi:10.4049/jimmunol.171.7.3855 [PubMed: 14500687]
28. Distler JHW, Schett G, Gay S, Distler O. The controversial role of tumor necrosis factor α in fibrotic diseases. Arthritis Rheum. 2008;58(8):2228–2235. doi:10.1002/art.23645 [PubMed: 18668576]
29. Mauviel A, Daireaux M, Rédini F, Galera P, Loyau G, Pujoi J-P. Tumor necrosis factor inhibits collagen and fibronectin synthesis in human dermal fibroblasts. FEBS Lett. 1988;236(1):47–52. doi:10.1016/0014-5793(88)80283-7 [PubMed: 3165348]
30. Miller JD, Weiss RM, Heistad DD. Calcific Aortic Valve Stenosis: Methods, Models, and Mechanisms. Towler DA, ed. Circ Res. 2011;108(11):1392–1412. doi:10.1161/CIRCRESAHA.110.234138 [PubMed: 21617136]
31. Weiss RM, Miller JD, Heistad DD. Fibrocalcific aortic valve disease: Opportunity to understand disease mechanisms using mouse models. Circ Res. 2013;113(2):209–222. doi:10.1161/CIRCRESAHA.113.300153 [PubMed: 23833295]
32. Cush JJ. Unusual toxicities with TNF inhibition: Heart failure and drug-induced lupus. Clin Exp Rheumatol. 2004;22(SUPPL. 35):S141–S147. Accessed June 21, 2019 https://www.clinexprheumatol.org/article.asp?a=2450 [PubMed: 15552528]
33. Antoni C, Braun J. Side effects of anti-TNF therapy: Current knowledge. Clin Exp Rheumatol. 2002;20(6 SUPPL. 28):S152–S157. Accessed June 21, 2019 https://www.clinexprheumatol.org/article.asp?a=1482 [PubMed: 12463468]
34. Sarzi-Puttini P, Atzeni F, Shoenfeld Y, Ferraccioli G. TNF-α, rheumatoid arthritis, and heart failure: A rheumatological dilemma. Autoimmun Rev. 2005;4(3):153–161. doi:10.1016/j.autrev.2004.09.004 [PubMed: 15823501]
35. Bradham WS, Moe G, Wendt KA, Scott AA, Konig A, Romanova M, Naik G, Spinale FG. TNF-α and myocardial matrix metalloproteinases in heart failure: relationship to LV remodeling. Am J Physiol Circ Physiol. 2002;282(4):H1288–H1295. doi:10.1152/ajpheart.00526.2001
36. Sinagra E, Perricone G, Romano C, Cottone M. Heart failure and anti tumor necrosis factor-alpha in systemic chronic inflammatory diseases. Eur J Intern Med. 2013;24(5):385–392. doi:10.1016/J.EJIM.2012.12.015 [PubMed: 23333028]
37. Dutka DP, Elborn JS, Delamere F, Shale DJ, Morris GK. Tumour necrosis factor alpha in severe congestive cardiac failure. Heart. 1993;70(2):141–143. doi:10.1136/hrt.70.2.141
38. Masjedi S, Lei Y, Patel J, Ferdous Z. Sex-related differences in matrix remodeling and early osteogenic markers in aortic valvular interstitial cells. Heart Vessels. 2017;32(2):217–228. doi:10.1007/s00380-016-0909-8 [PubMed: 27761653]
39. Parhami F, Basseri B, Hwang J, Tintut Y, Demer LL. High-Density Lipoprotein Regulates Calcification of Vascular Cells. Circ Res. 2002;91(7):570–576. doi:10.1161/01.RES.0000036607.05037.DA [PubMed: 12364384]
40. Bowler MA, Merryman WD. In vitro models of aortic valve calcification: solidifying a system. Cardiovasc Pathol. 2015;24(1):1–10. doi:10.1016/J.CARPATH.2014.08.003 [PubMed: 25249188]
41. Hjortnaes J, Goettsch C, Hutcheson JD, Camci-Unal G, Lax L, Scherer K, Body S, Schoen FJ, Kluin J, Khademhosseini A, Aikawa E. Simulation of Early Calcific Aortic Valve Disease in a 3D platform: A Role for Myofibroblast Differentiation HHS Public Access. J Mol Cell Cardiol. 2016;94:13–20. doi:10.1016/j.yjmcc.2016.03.004 [PubMed: 26996755]
42. Galeone A, Brunetti G, Oranger A, Greco G, Di Benedetto A, Mori G, Colucci S, Zallone A, Paparella D, Grano M. Aortic valvular interstitial cells apoptosis and calcification are mediated by TNF-related apoptosis-inducing ligand. Int J Cardiol. 2013;169(4):296–304. doi:10.1016/J.IJCARD.2013.09.012 [PubMed: 24148916]
43. Moreno PR, Astudillo L, Elmariah S, Purushothaman KR, Purushothaman M, Lento PA, Sharma SK, Fuster V, Adams DH. Increased macrophage infiltration and neovascularization in congenital bicuspid aortic valve stenosis. J Thorac Cardiovasc Surg. 2011;142(4):895–901. doi:10.1016/j.jtcvs.2011.03.002 [PubMed: 21481422]

44. Wang R, Chen W, Ma Z, Li L, Chen X. M1/M2 macrophages and associated mechanisms in congenital bicuspid aortic valve stenosis. Exp Ther Med. 2014;7(4):935–940. doi:10.3892/etm.2014.1529 [PubMed: 24669254]
45. Segura AM, Frazier OH, Buja LM. Fibrosis and heart failure. Heart Fail Rev. 2014;19(2):173–185. doi:10.1007/s10741-012-9365-4 [PubMed: 23124941]
46. Garcia D, Pibarot P, Dumesnil JG, Sakr F, Durand LG. Assessment of aortic valve stenosis severity: A new index based on the energy loss concept. Circulation. 2000;101(7):765–771. doi:10.1161/01.CIR.101.7.765 [PubMed: 10683350]
47. Minners J, Allgeier M, Gohlke-Baerwolf C, Kienzle R-P, Neumann F-J, Jander N. Inconsistencies of echocardiographic criteria for the grading of aortic valve stenosis. Eur Heart J. 2008;29:1043–1048. doi:10.1093/eurheartj/ehn080 [PubMed: 18156619]
48. Lehmkuhl L, Foldyna B, Von Aspern K, Lücke C, Grothoff M, Nitzsche S, Kempfert J, Haensig M, Rastan A, Walther T, Mohr FW, Gutberlet M. Inter-individual variance and cardiac cycle dependency of aortic root dimensions and shape as assessed by ECG-gated multi-slice computed tomography in patients with severe aortic stenosis prior to transcatheter aortic valve implantation: Is it crucial for correct sizing? Int J Cardiovasc Imaging. 2013;29(3):693–703. doi:10.1007/s10554-012-0123-4 [PubMed: 22986896]
49. Mabry KM, Payne SZ, Anseth KS. Microarray analyses to quantify advantages of 2D and 3D hydrogel culture systems in maintaining the native valvular interstitial cell phenotype. Biomaterials. 2016;74:31–41. doi:10.1016/j.biomaterials.2015.09.035 [PubMed: 26433490]
50. Fairbanks BD, Schwartz MP, Halevi AE, Nuttelman CR, Bowman CN, Anseth KS. A versatile synthetic extracellular matrix mimic via thiol-norbornene photopolymerization. Adv Mater. 2009;21(48):5005–5010. doi:10.1002/adma.200901808 [PubMed: 25377720]
51. Schindelin J, Arganda-Carreras I, Frise E, Kaynig V, Longair M, Pietzsch T, Preibisch S, Rueden C, Saalfeld S, Schmid B, Tinevez JY, White DJ, Hartenstein V, Eliceiri K, Tomancak P, Cardona A. Fiji: An open-source platform for biological-image analysis. Nat Methods. 2012;9(7):676–682. doi:10.1038/nmeth.2019 [PubMed: 22743772]
52. Gonzalez Rodriguez A, Schroeder ME, Walker CJ, Anseth KS. FGF-2 inhibits contractile properties of valvular interstitial cell myofibroblasts encapsulated in 3D MMP-degradable hydrogels. APL Bioeng. 2018;2(4):046104. doi:10.1063/1.5042430 [PubMed: 31069326]
53. Yadav M, Kamath KR, Iyngkaran N, Sinniah M. Dengue haemorrhagic fever and dengue shock syndrome: are they tumour necrosis factor-mediated disorders? FEMS Microbiol Immunol. 1991;89:45–50. doi:10.1111/j.1574-6968.1991.tb04969.x
54. Linderholm M, Ahlm C, Settergren B, Waage A, Tärnvik A. Elevated plasma levels of tumor necrosis factor (TNF)-α, soluble TNF receptors, interleukin (IL)-6, and IL-10 in patients with hemorrhagic fever with renal syndrome. J Infect Dis. 1996;173(1):38–43. doi:10.1093/infdis/173.1.38 [PubMed: 8537680]
55. Sorimachi K, Akimoto K, Hattori Y, Ieiri T, Niwa A. Activation of macrophages by lactoferrin: secretion of TNF-α, IL-8 and NO. Biochem Mol Biol Int. 1997;43(1):79–87. doi:10.1080/15216549700203841 [PubMed: 9315285]
56. Dutka DP, Elbom JS, Delamere F, Shale DJ, Morris GK, Hospital C, P Dutka JS, Elbom F, Delamere DJ, Shale GK, Morris ND. Tumour necrosis factor alpha in severe congestive cardiac failure. Br Hear. 1993;70:141–143. doi:10.1136/hrt.70.2.141
57. Fahey TJ, Sherry B, Tracey KJ, van Deventer S, Jones WG, Minei JP, Morgello S, Shires GTT, Cerami A. Cytokine production in a model of wound healing: The appearance of MIP-1, MIP-2, cachectin/TNF and IL-I. Cytokine. 1990;2(2):92–99. doi:10.1016/1043-4666(90)90002-B [PubMed: 2104219]
58. Fràter-Schröder M, Risau W, Hallmann R, Gautschi P, Böhlen P. Tumor necrosis factor type alpha, a potent inhibitor of endothelial cell growth in vitro, is angiogenic in vivo. Proc Natl Acad Sci U S A. 1987;84(15):5277–5281. doi:10.1073/pnas.84.15.5277 [PubMed: 2440047]
59. Galeone A, Paparella D, Colucci S, Grano M, Brunetti G, Awano K, Lobdell KW, Misumi I. The Role of TNF-a and TNF Superfamily Members in the Pathogenesis of Calcific Aortic Valvular Disease. Sci World J. Published online 2013. doi:10.1155/2013/875363

60. Sabio G, Davis RJ. TNF and MAP kinase signalling pathways. Semin Immunol. 2014;26(3):237–245. doi:10.1016/j.smim.2014.02.009 [PubMed: 24647229]
61. Orgaz JL, Crosas-Molist E, Sadok A, Perdrix-Rosell A, Maiques O, Rodriguez-Hernandez I, Monger J, Mele S, Georgouli M, Bridgeman V, Karagiannis P, Lee R, Pandya P, Boehme L, Wallberg F, Tape C, Karagiannis SN, Malanchi I, Sanz-Moreno V. Myosin II Reactivation and Cytoskeletal Remodeling as a Hallmark and a Vulnerability in Melanoma Therapy Resistance. Cancer Cell. 2020;37(1):85–103.e9. doi:10.1016/j.ccell.2019.12.003 [PubMed: 31935375]
62. Yu Z, Seya K, Daitoku K, Motomura S, Fukuda I, Furukawa KI. Tumor necrosis factor-α accelerates the calcification of human aortic valve interstitial cells obtained from patients with calcific aortic valve stenosis via the BMP2-Dlx5 pathway. J Pharmacol Exp Ther. 2011;337(1):16–23. doi:10.1124/jpet.110.177915 [PubMed: 21205918]
63. Tintut Y, Patel J, Parhami F, Demer LL. Tumor necrosis factor-α promotes in vitro calcification of vascular cells via the cAMP pathway. Circulation. 2000;102(21):2636–2642. doi:10.1161/01.CIR.102.21.2636 [PubMed: 11085968]
64. Aguado BA, Schuetze KB, Grim JC, Walker CJ, Cox AC, Ceccato TL, Tan A-C, Sucharov CC, Leinwand LA, Taylor MRG, Mckinsey TA, Anseth KS. Transcatheter aortic valve replacements alter circulating serum factors to mediate myofibroblast deactivation. Sci Transl Med. 2019;11:3233 Accessed March 24, 2020 http://stm.sciencemag.org/
65. Duan B, Yin Z, Hockaday Kang L, Magin RL, Butcher JT. Active tissue stiffness modulation controls valve interstitial cell phenotype and osteogenic potential in 3D culture. Acta Biomater. 2016;36:42–54. doi:10.1016/j.actbio.2016.03.007 [PubMed: 26947381]
66. Liu AC, Joag VR, Gotlieb AI. The emerging role of valve interstitial cell phenotypes in regulating heart valve pathobiology. Am J Pathol. 2007;171(5):1407–1418. doi:10.2353/ajpath.2007.070251 [PubMed: 17823281]
67. Yip CYY, Simmons CA. The aortic valve microenvironment and its role in calcific aortic valve disease. Cardiovasc Pathol. 2011;20(3):177–182. doi:10.1016/j.carpath.2010.12.001 [PubMed: 21256052]
68. Lim J, Ehsanipour A, Hsu JJ, Lu J, Pedego T, Wu A, Walthers CM, Demer LL, Seidlits SK, Tintut Y. Inflammation Drives Retraction, Stiffening, and Nodule Formation via Cytoskeletal Machinery in a Three-Dimensional Culture Model of Aortic Stenosis. Am J Pathol. 2016;186(9):2378–2389. doi:10.1016/J.AJPATH.2016.05.003 [PubMed: 27392969]
69. Ho AL, Grewal RK, Leboeuf R, Sherman EJ, Pfister DG, Deandreis D, Pentlow KS, Zanzonico PB, Haque S, Gavane S, Ghossein RA, Ricarte-Filho JC, Domínguez JM, Shen R, Tuttle RM, Larson SM, Fagin JA. Sel-u-me-ti-nib-Enhanced- Radioiodine- Uptake- in Advanced -Thyroid -Cancer. n engl j med. 2013;7:623–655. doi:10.1056/NEJMoa1209288
70. Casaluce F, Sgambato A, Maione P, Sacco PC, Santabarbara G, Gridelli C. Selumetinib for the treatment of non-small cell lung cancer. Expert Opin Investig Drugs. 2017;26(8):973–984. doi:10.1080/13543784.2017.1351543
71. Do K, Speranza G, Bishop R, Khin S, Rubinstein L, Kinders RJ, Datiles M, Eugeni M, Lam MH, Doyle LA, Doroshow JH, Kummar S. Biomarker-driven phase 2 study of MK-2206 and selumetinib (AZD6244, ARRY-142886) in patients with colorectal cancer. Invest New Drugs. 2015;33(3):720–728. doi:10.1007/s10637-015-0212-z [PubMed: 25637165]
72. Dombi E, Baldwin A, Marcus LJ, Fisher MJ, Weiss B, Kim A, Whitcomb P, Martin S, Aschbacher-Smith LE, Rizvi TA, Wu J, Ershler R, Wolters P, Therrien J, Glod J, Belasco JB, Schorry E, Brofferio A, Starosta AJ, Gillespie A, Doyle AL, Ratner N, Widemann BC. Activity of Selumetinib in Neurofibromatosis Type 1–Related Plexiform Neurofibromas. N Engl J Med. 2016;375(26):2550–2560. doi:10.1056/NEJMoa1605943 [PubMed: 28029918]
73. Muchir A, Reilly SA, Wu W, Iwata S, Homma S, Le Bonne G, Worman HJ. Treatment with selumetinib preserves cardiac function and improves survival in cardiomyopathy caused by mutation in the lamin A/C gene. Cardiovasc Res. 2012;93:311–319. doi:10.1093/cvr/cvr301 [PubMed: 22068161]
74. Wang B, Yao K, Wise AF, Lau R, Shen HH, Tesch GH, Ricardo SD. miR-378 reduces mesangial hypertrophy and kidney tubular fibrosis via MAPK signalling. Clin Sci. 2017;131(5):411–423. doi:10.1042/CS20160571

75. Zhan Q, Song R, Zeng Q, Yao Q, Ao L, Xu D, Fullerton DA, Meng X. Activation of TLR3 induces osteogenic responses in human aortic valve interstitial cells through the NF-κB and ERK1/2 pathways. Int J Biol Sci. 2015;11(4):482–493. doi:10.7150/ijbs.10905 [PubMed: 25798067]

76. Rutkovskiy A, Malashicheva A, Sullivan G, Bogdanova M, Kostareva A, Stensløkken; Are-Olav K, Fiane A, Vaage J. Valve Interstitial Cells: The Key to Understanding the Pathophysiology of Heart Valve Calcification. J Am Heart Assoc. 2017;6(9). doi:10.1161/JAHA.117.006339

77. He C, Tang H, Mei Z, Li N, Zeng Z, Darko KO, Yin Y, Hu CAA, Yang X. Human interstitial cellular model in therapeutics of heart valve calcification. Amino Acids. 2017;49(12):1981–1997. doi:10.1007/s00726-017-2432-3 [PubMed: 28536843]

78. Zeng Q, Song R, Ao L, Weyant MJ, Lee J, Xu D, Fullerton DA, Meng X. Notch1 promotes the pro-osteogenic response of human aortic valve interstitial cells via modulation of erk1/2 and nuclear factor-κb activation. Arterioscler Thromb Vasc Biol. 2013;33(7):1580–1590. doi:10.1161/ATVBAHA.112.300912 [PubMed: 23640488]

79. Li C, Gotlieb AI. Transforming growth factor-β regulates the growth of valve interstitial cells in vitro. Am J Pathol. 2011;179(4):1746–1755. doi:10.1016/j.ajpath.2011.06.007 [PubMed: 21851806]

80. Strutz F, Zeisberg M, Renziehausen A, Raschke B, Becker V, Van Kooten C, Müller GA. TGF-β1 induces proliferation in human renal fibroblasts via induction of basic fibroblast growth factor (FGF-2). Kidney Int. Published online 2001. doi:10.1046/j.1523-1755.2001.059002579.x

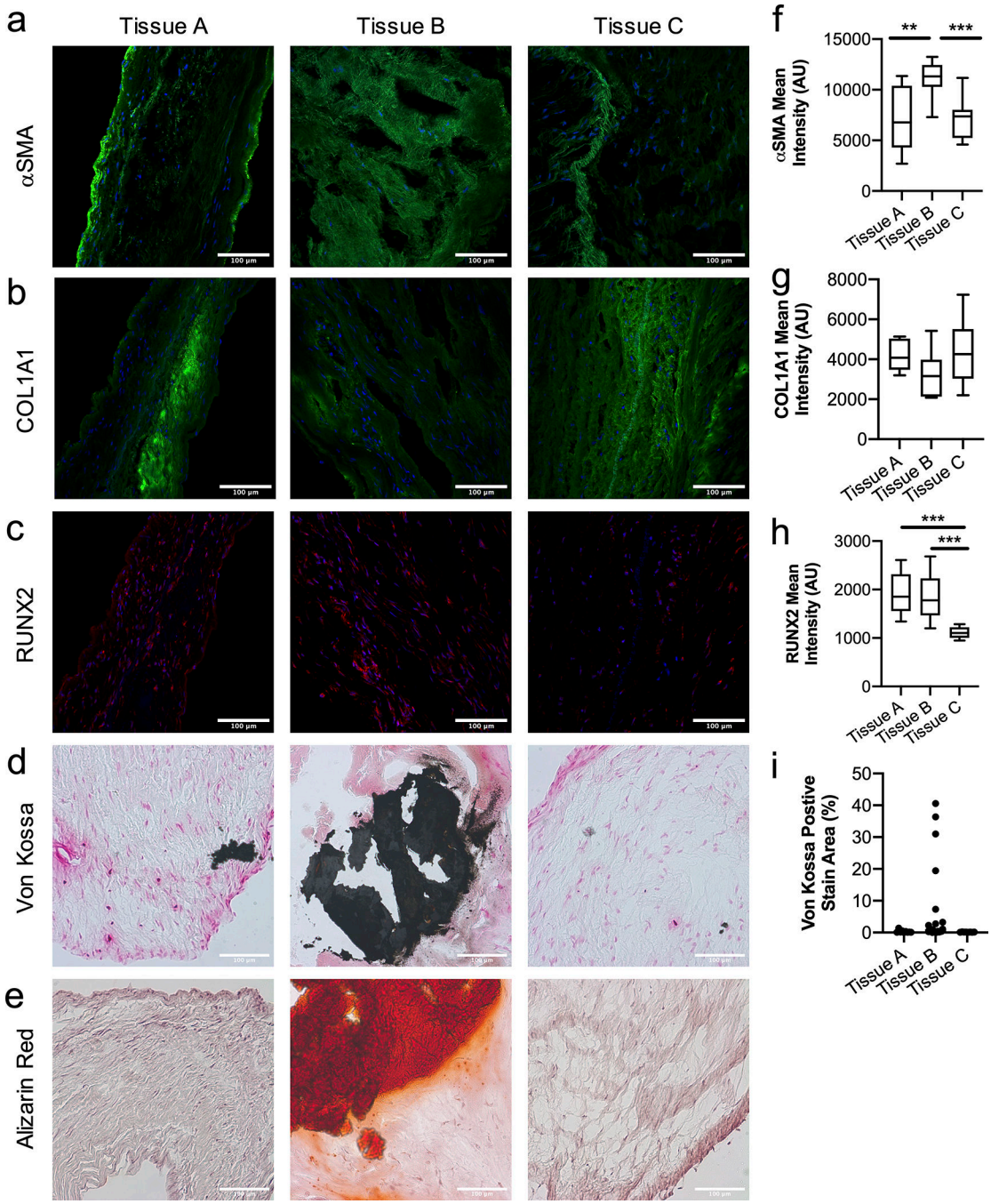

Figure 1. Human valve tissue from male patients with valve disorder present a high degree of variability and heterogeneity in the fibroblast and myofibroblast cell population.

a-e) Histological sections of aortic valve tissue from male patients diagnosed with heart valve disorder. Immunostaining for fibrotic markers, a) αSMA and b) COL1A1 (green, nucleus in blue), show high variability between tissues and heterogeneity in the fibroblast and myofibroblast population, indicated by αSMA staining. Calcific markers, c) RUNX2 (red, nucleus in blue), d) Von Kossa (calcium phosphate in black) and e) Alizarin Red (calcium in red) demonstrate high variability in tissue mineralization. Scale bars=100μm. Quantification of f) αSMA g) COL1A1 and h) RUNX2 intensity analysis for tissue sections,

significant differences are observed between tissues for αSMA and RUNX2. i) Quantification of area percentage of Von Kossa positive stain (black) indicates variability of calcification between tissues. Statistical analysis was performed on fields of view for each biological replicate (n≥10 images per biological replicate), ***=p<0.001 and **=p<0.01 based on one-way ANOVA.

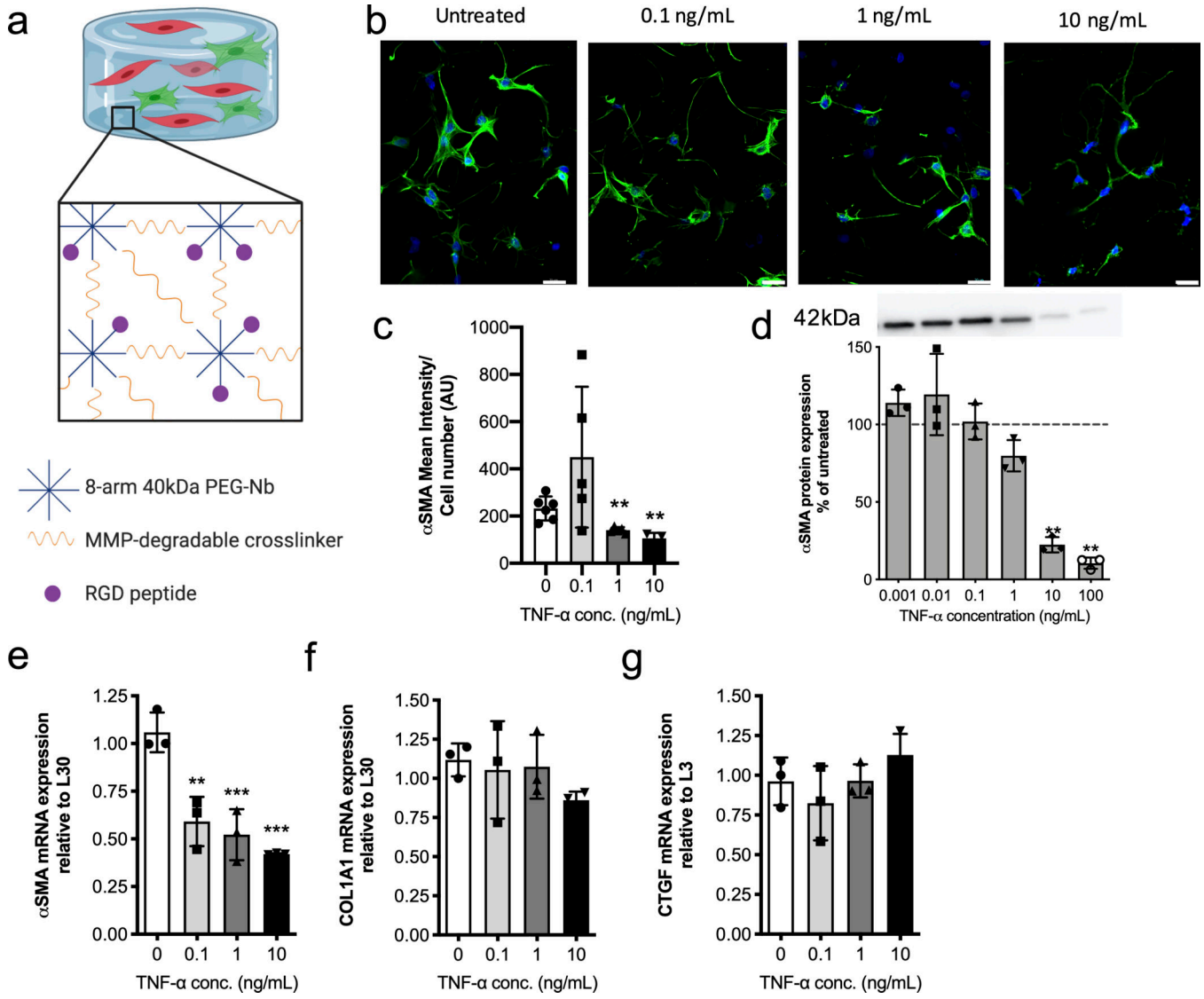

Figure 2. Encapsulated VICs respond to TNF-α treatment with a decrease in expression of fibrotic markers.

a) Schematic of 3D hydrogel culture platform. 8-arm 40kDa PEG-norbornene is reacted with an MMP-degradable dithiol crosslinker and RGD adhesive peptide is added to allow for VIC-matrix interactions. b) Representative immunostaining images of VICs treated with growth media (untreated) and 0.1, 1, or 10 ng/mL of TNF-α treatment. αSMA stress fibers (green) formation decreases with increasing TNF-α treatment concentration. Nucleus (blue) and αSMA (green). Scale bars=20μm. c) αSMA mean intensity analysis with respect to cell number for VICs in untreated and 0.1, 1, or 10 ng/mL TNF-α treatment conditions. TNF-α treatment resulted in a significant decrease in αSMA mean intensity at higher doses. d) VIC αSMA protein expression normalized to untreated controls (dotted line) and measured via western blot. A representative western blot used for analysis (top) where all lanes are from the same blot. αSMA protein expression significantly decreases with increasing TNF-α concentration. e-g) mRNA gene expression levels relative to L30 for the fibrotic markers e) αSMA f) COL1A1 and the fibroblast marker g) CTGF. Increasing treatment with TNF-α

results in significant downregulation in αSMA gene expression, while COL1A1 gene expression shows a decreasing trend, albeit not statistically significant. CTGF gene expression was slightly increased with TNF-α treatment, but no significant differences were observed. ***=$p<0.001$ and **=$p<0.01$, based on one-way ANOVA.

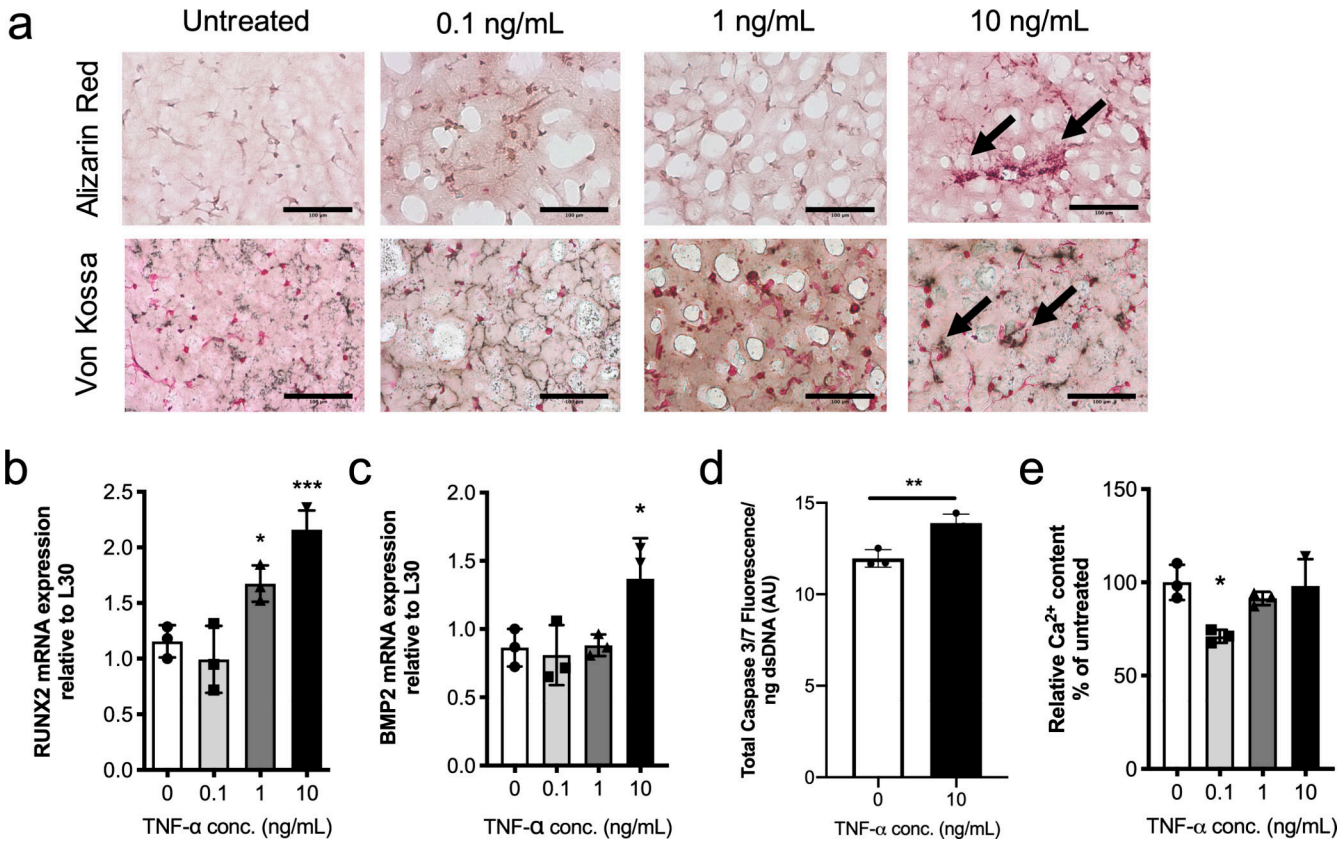

Figure 3. TNF-α treatment promotes the VIC osteoblast-like phenotype and matrix calcification.

a) Representative images from 3D cryosectioned samples stained with Alizarin Red (top) and Von Kossa (bottom) for untreated conditions and 0.1, 1, and 10 ng/mL TNF-α. Increasing TNF-α treatment leads to an increase in Alizarin Red (red) and Von Kossa (black) staining. Scale bars=100μm. b,c) mRNA gene expression levels relative to L30 for calcific markers b) RUNX2 and c) BMP2. Both RUNX2 and BMP2 gene expression were significantly upregulated relative to untreated with 10 ng/mL of TNF-α. d) Quantification of Caspase 3 fluorescence signal normalized with dsDNA content. Caspase 3 fluorescence shows a significantly increased in VICs treated with TNF-α compared to untreated samples. e) Deposited calcium signal normalized to dsDNA content and expressed as percent of untreated control (0 ng/mL of TNF-α). No trends were observed with TNF-α treatment, although significantly reduced calcium content was observed with 0.1 ng/mL of TNF-α. ***=$p<0.001$, **=$p<0.01$ and **=$p<0.05$ based on one-way ANOVA and t-test.

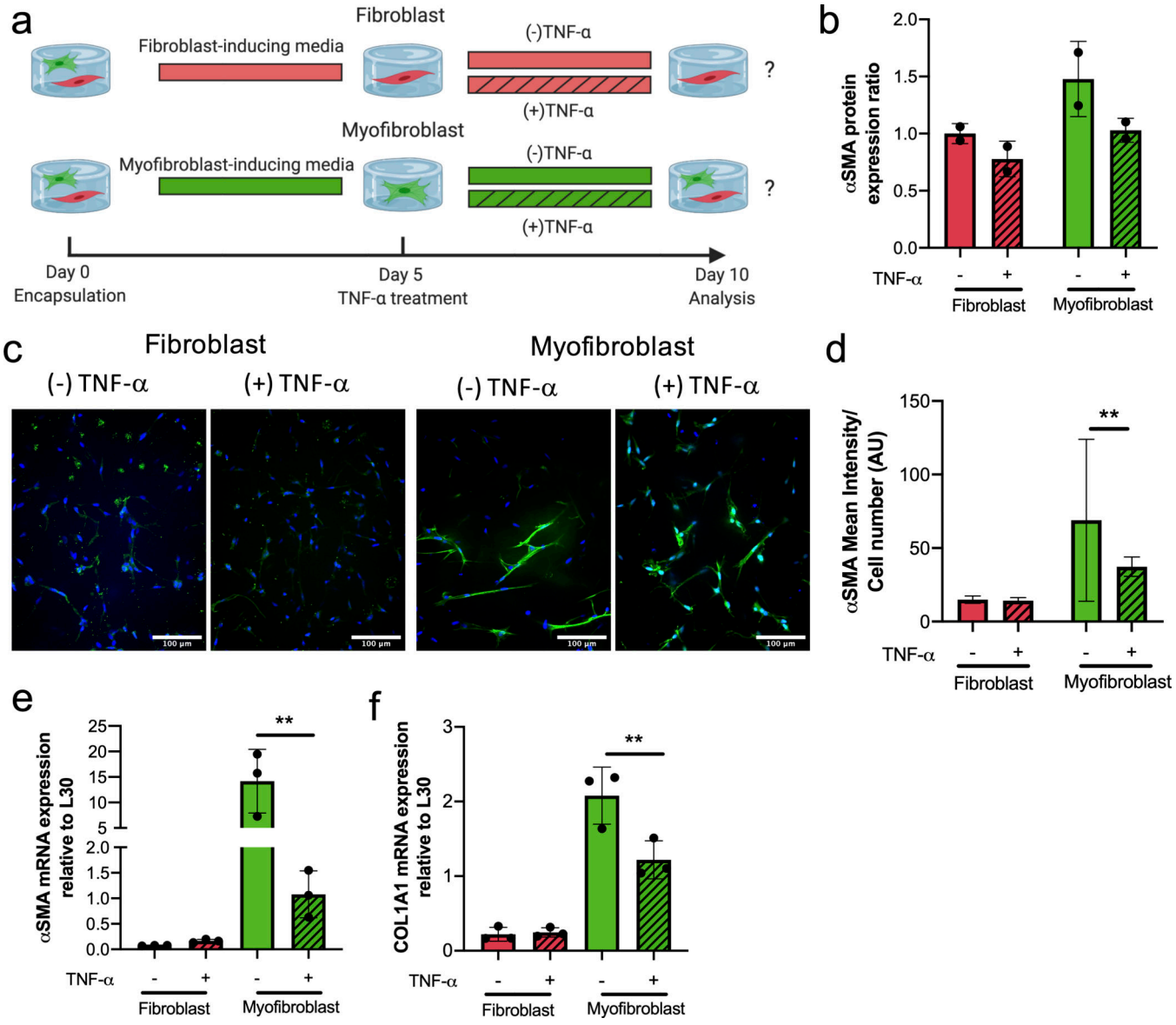

Figure 4. VIC myofibroblast populations respond to TNF-α treatment by decreasing their fibrotic markers.

a) Experimental design to investigate the effects of TNF-α (10 ng/mL) treatment on defined VIC fibroblast or activated myofibroblast populations. b) αSMA protein expression ratio for fibroblast (red) and activated myofibroblast (green) phenotypes in the presence or absence of TNF-α. αSMA protein expression decreases with the addition of TNF-α (patterned) on both fibroblasts and activated myofibroblast. c) Representative immunostaining images for αSMA stress fibers of fibroblasts and activated myofibroblast in the presence or absence of TNF-α. Nucleus (blue) and αSMA (green). Scale bars=100μm. d) Intensity analysis of αSMA normalized to cell number results in a significant decrease in αSMA mean intensity for activated myofibroblast treated with 10 ng/mL of TNF-α. No change in intensity was observed in VIC fibroblasts treated with 10 ng/mL of TNF-α. e) αSMA and f) COL1A1 mRNA gene expression levels relative to L30. Fibroblast populations treated with 10 ng/mL

TNF-α had no significant changes in gene expression of αSMA and COL1A1 relative to untreated fibroblasts. Activated myofibroblast populations treated with TNF-α resulted in a significant downregulation of αSMA and COL1A1 gene expression. **=p<0.01 based on t-test.

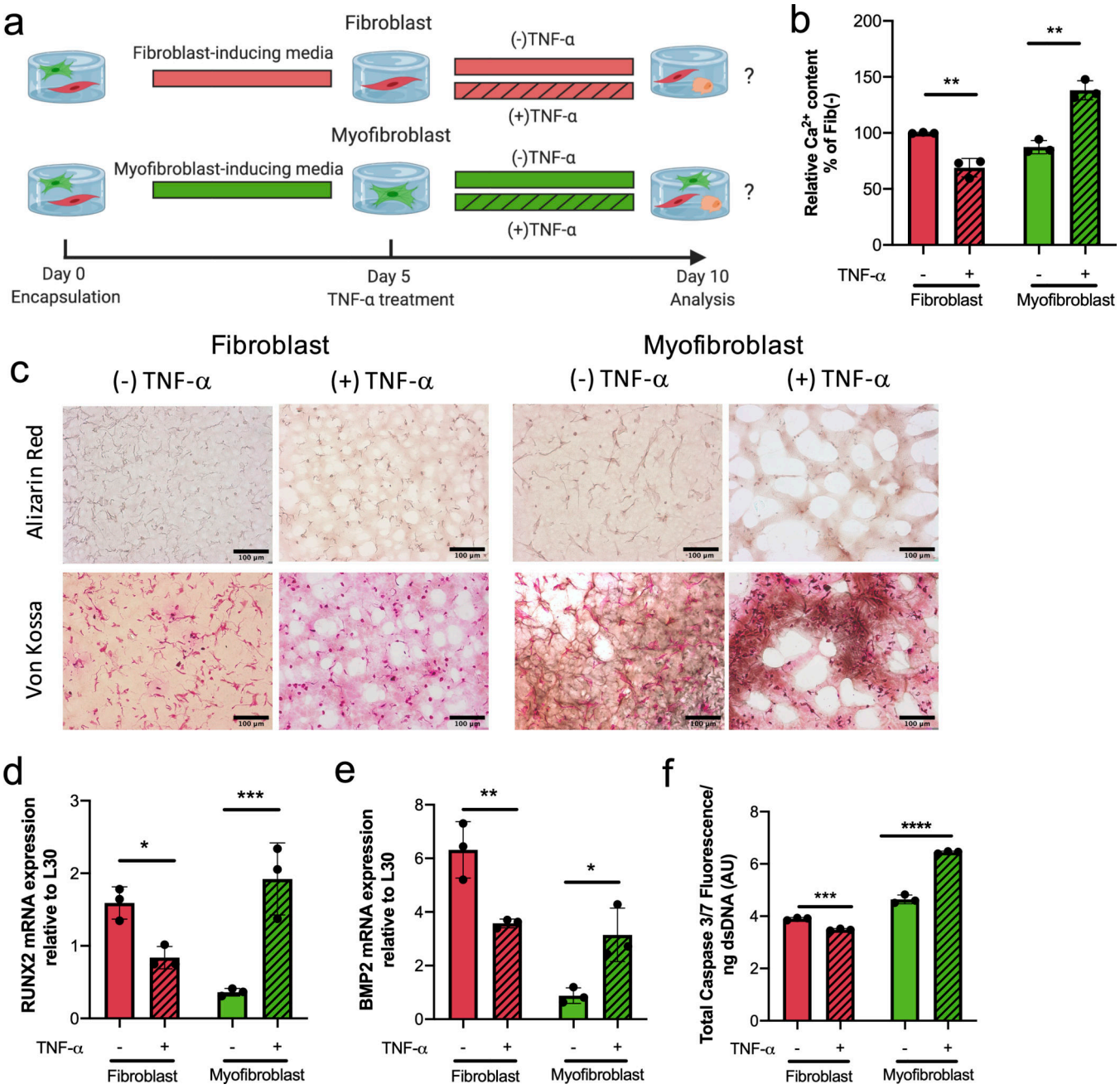

Figure 5. Myofibroblasts treated with TNF-α have a calcific response whereas fibroblasts decrease expression of calcific markers.

a) Experimental set up to investigate the effects of TNF-α (10 ng/mL) on defined fibroblast and activated myofibroblast populations to assess calcific markers. b) Quantification of deposited calcium signal normalized to dsDNA content and expressed as percent of untreated fibroblast control (0 ng/mL of TNF-α). A significant decrease of deposited calcium was observed with fibroblasts (red) treated with TNF-α (patterned), while the opposite trend was observed with activated myofibroblast (green) resulting in a significant increase of calcium with TNF-α treatment. c) Representative images from cryosectioned samples stained with Alizarin Red (top) and Von Kossa (bottom) for activated myofibroblast

and fibroblast populations in the presence or absence of TNF-α. Fibroblasts had no positive stain for either calcific marker and treatment with TNF-α had no effect on either stain. The activated myofibroblast phenotype presented minimal positive Von Kossa and Alizarin Red stain but addition of TNF-α treatment resulted in exacerbated increase of positive staining for both stains. Scale bars=100μm. d) RUNX2 and e) BMP2 mRNA gene expression levels relative to L30. Both calcific markers, RUNX2 and BMP2, gene expression was downregulated on fibroblasts treated with TNF-α. Activated myofibroblast treated with TNF-α resulted in significant upregulation of both RUNX2 and BMP2 gene expression. f) Caspase 3 fluorescence signal normalized to dsDNA content. Activated myofibroblast treated with TNF-α had a significant increase in Caspase 3 fluorescence, while fibroblasts resulted in a significant decrease of Caspase 3 in the presence of TNF-α. ****=$p<0.0001$, ***=$p<0.001$, **=$p<0.01$ and **=$p<0.05$ based on t-test.

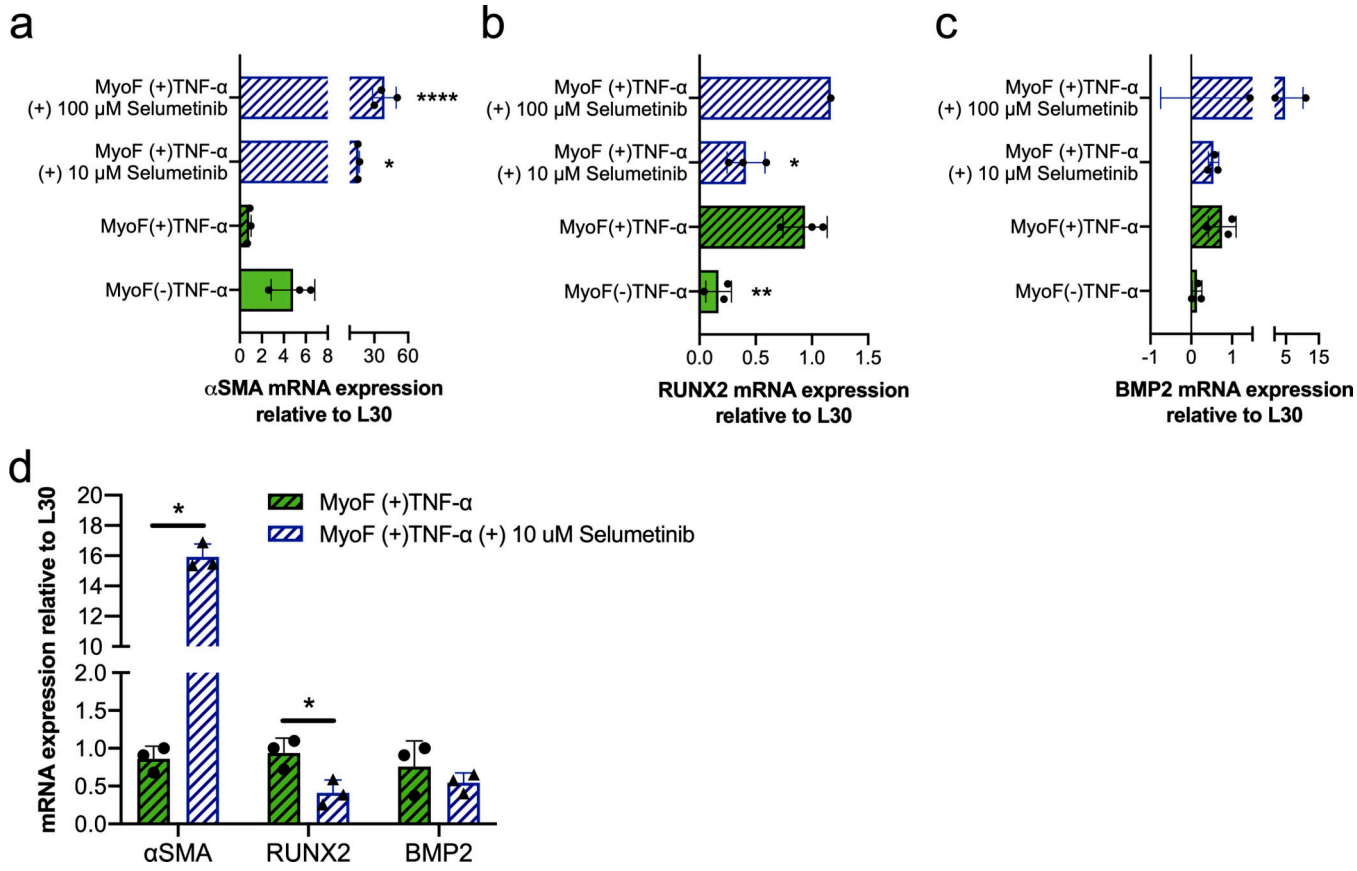

Figure 6. The MAPK/ERK pathway is involved in the VIC activated myofibroblast calcific response to TNF-α.

a) αSMA b) RUNX2 and c) BMP2 mRNA gene expression relative to L30. Activated myofibroblast populations were treated with TNF-α or left untreated. TNF-α-treated activated myofibroblast were cultured in the presence or absence of Selumetinib. Selumetinib resulted in significant upregulation of αSMA gene expression at both concentrations. RUNX2 gene expression was significantly reduced with low dose of Selumetinib (10 uM) but no statistically different changes on BMP2 gene expression were observed with either dose. d) Comparative results of mRNA gene expression for αSMA, RUNX2, and BMP2 of TNF-α-treated activated myofibroblast with and without low dose of Selumetinib (10 mM). Comparative results showcase αSMA gene expression was 18.5-fold higher with Selumetinib (10 mM), RUNX2 gene expression was reduced by half and BMP2 was not significantly altered. ****=p<0.0001, ***=p<0.001 and **=p<0.05 based on one-way ANOVA and t-test.

Table 1.

Custom primer sequences.

Gene	Forward primer (5’-3’)	Reverse primer (5’-3’)
L30	AGATTTCCTCAAGGCTGGGC	GCTGGGGTACAAGCAGACTC
α-SMA	GCAAACAGGAATACGATGAAGCC	AACACATAGGTAACGAGTCAGAGC
CTGF	CTGGTCCAGACCACAGAGTGG	GCAGAAAGCGTTGTCATTGG
COL1A1	GGGCAAGACAGTGATTGAATACA	GGATGGAGGGAGTTTACAGGAA
RUNX2	AACAACCACAGAACCACAAG	TGACCTGCGGAGATTAACC
BMP2	TCTACGAAAAGAAGTTGGGAAAACA	TACTTCATGTGCTGGGGTTGA